Acousto-optic replication of ultrashort laser pulses

Konstantin B. Yushkov* and Vladimir Ya. Molchanov
National University of Science and Technology "MISIS", 4 Leninsky Prospekt, Moscow 119049, Russia

Andrey V. Ovchinnikov and Oleg V. Chefonov
Joint Institute for High Temperatures of the Russian Academy of Sciences, Izhorskaya 13, Building 2, Moscow 125412, Russia
(Received 2 August 2017; published 30 October 2017)

Precisely controlled sequences of ultrashort laser pulses are required in various scientific and engineering applications. We developed a phase-only acousto-optic pulse shaping method for replication of ultrashort laser pulses in a TW laser system. A sequence of several Fourier-transform-limited pulses is generated from a single femtosecond laser pulse by means of applying a piecewise linear phase modulation over the whole emission spectrum. Analysis demonstrates that the main factor which limits maximum delay between the pulse replicas is spectral resolution of the acousto-optic dispersive delay line used for pulse shaping. In experiments with a Cr:forsterite laser system, we obtained delays from 0.3 to 3.5 ps between two replicas of 190 fs transform-limited pulses at the central wavelength of laser emission, 1230 nm.

DOI: 10.1103/PhysRevA.96.043866

I. INTRODUCTION

In recent decades, femtosecond laser technology has grown into a mature field, providing a variety of commercially available lasers for a broad scope of users. The state of the art in ultrafast optics includes few-cycle master oscillators, adaptive pulse shaping systems, bench-top multi-TW amplifiers, and a variety of pulse characterization instruments. An essential branch of ultrafast optics is pulse shaping. General principles and methods of ultrashort pulse shaping can be found in a review by Weiner [1]. Usually, a required temporal shape of ultrashort pulses delivered to the target is specified by application.

One of the problems of temporal pulse shaping is to synthesize a given number of ultrashort laser pulses from a single pulse with controlled delays, amplitudes, and phases. Precisely controlled sequences of ultrashort laser pulses are required in many scientific and engineering applications: atomic and molecular dynamics control [2,3], time-resolved molecular spectroscopy [4], wakefield electron accelerators [5], quantum experiments [6,7], selective excitation of multiphoton fluorescence [8], laser ablation [9,10], Raman lasers [11–13], coherent synthesis of laser pulses [14], etc. One of the most relevant applications of ultrashort laser pulse replicas is generation of tunable THz radiation [15–18]. Adaptive pulse replication can be also used for self-referenced characterization of ultrashort pulses [19,20]. From the pulse-shaping point of view, the particular problem is to create a specific phase and/or amplitude modulation in the spectral domain by the pulse shaper providing the multi-peak pulse envelope at the output.

Several application schemes of adaptive pulse shapers in chirped pulse amplification (CPA) and optical parametric amplification systems are known. When a shaper is placed before the amplifiers, it performs phase and spectral predistortions of pulses [21–24]. A nonlinear response of output emission parameters to pulse shaping is usually observed in this configuration because of pulse distortions in amplifiers. Compensation of gain narrowing in regenerative amplifiers can be efficiently obtained when a spectral pulse shaper is placed in the amplifier cavity [25,26]. When high contrast of spectral modulation is specially required, a pulse shaper can be located between preamplifier stages and final power amplifiers [27,28]. Finally, a pulse shaper can be placed after all amplifier stages, but the losses in the shaper cannot be compensated in this case [29]. A choice of laser system architecture is usually defined by the application and required pulse parameters.

In this paper we developed a method for producing ultrashort pulse sequences in a CPA terawatt laser system using acousto-optic (AO) pulse shaping in the front-end part of the laser. AO tunable filters (AOTFs) are used in classical spectroscopy, providing useful features of fast random-access wavelength tuning, high numerical aperture, reliability, compactness, and light weight [30]. Feeding an AO filter with synthesized broadband signals enables new applications such as ultrashort pulse compression and shaping [21,24,31–34] and matched spectral processing of incoherent light [35]. Spectral transmission function of an AO filter is complex valued, i.e., it affects both phase and magnitudes of spectral components of transmitted light. This feature is used for generating femtosecond pulse sequences.

A linear pulse shaper can be described with a complex-valued transmission function $\widetilde{H}(\omega)$ which couples the input and the output spectra:

$$\widetilde{S}_{\text{out}}(\omega) = \widetilde{S}_{\text{in}}(\omega)\widetilde{H}(\omega). \tag{1}$$

Hereinafter we use the tilde for complex-valued functions of real variables. The transmission function $\widetilde{H}(\omega)$ is defined on a finite frequency interval $\Delta\omega$.

A trivial solution to the pulse replication problem is to use the following transmission function of the shaper:

$$\widetilde{H}(\omega) = \sum_{n=1}^{N} A_n \exp(i\omega\tau_n). \tag{2}$$

The fourier transform of the output spectrum $\widetilde{S}_{\text{out}}(\omega)$ obtained with the transmission function (2) will be a sequence of

*Corresponding author: konstantin.yushkov@misis.ru

N pulses similar to the input one with amplitudes A_n and relative delays τ_n. However, an ideal transmission function $\widetilde{H}(\omega)$ described by Eq. (2) is affected in experiment by limited contrast and resolution of the shaper. Several results of pulse replica generation with this method using AO time-domain shaping were reported in Refs. [21,29,36–38]; however, the analysis has not been performed in full.

As mentioned above, the most common application scheme is to use the pulse shaper before amplifier stages. In this case, inevitable energy loss in the shaper can be compensated by increasing the amplifier gain. On the other hand, gain saturation in amplifiers can reduce modulation contrast that results in degradation of the pulse sequence or appearance of undesired pre- and post-pulses. This a common case for regenerative amplifiers running in saturated regime. For this reason, phase-only pulse shaping techniques can be preferable for using a shaper in the front end of a laser system. Those methods rely on providing a complicated phase modulation with constant absolute value of the spectral transmission $|\widetilde{H}(\omega)| = 1$.

Several phase-only pulse shaping methods have been developed for spatial light modulators [39–42]. The algorithms of pulse shaping were specified for liquid crystal spatial light modulators having a discrete pixelized structure. In contrast, the optical spectrum in AO pulse shaping is treated as a continuum that increases flexibility of signal encoding algorithms.

Here we present analysis and experimental performance of a phase-only pulse shaping technique provided by an acousto-optic (AO) method for synthesis of femtosecond pulse sequences. The absence of amplitude modulation at the output of the shaper results in a higher energy of output pulses than obtained using conventional phase-and-amplitude pulse shaping. The experiments were performed with a Cr:forsterite terawatt laser and demonstrated feasibility of phase-only AO pulse shaping for generation of accurately controlled pulse replicas.

II. METHOD DESCRIPTION AND ANALYSIS

A. General form of transmission function

In an acousto-optic dispersive delay line (AODDL), a dynamic chirped Bragg grating is created by ultrasound in a birefringent crystal providing an arbitrary complex-valued transmission function $\widetilde{H}(\omega)$ [24,31,32]. Ultrasonic waveforms are synthesized with a radio frequency (RF) arbitrary waveform generator (AWG). A single AODDL is capable of phase-and-amplitude modulation if the first diffraction order is used as the output beam. Central optical frequency ω_0, passband $\Delta\omega$, and dispersion of diffracted light are controlled electronically by adjustment of ultrasonic waveform parameters [33].

Transmission function of a pulse shaper providing a sequence of N pulses at the output can be presented in a general form,

$$\widetilde{H}(\omega) = T(\omega)\sum_{n=1}^{N} A_n M_n(\omega) \times \exp\left[i\omega\tau_n + i\sum_{k\geqslant 2} D_n^{(k)}(\omega-\omega_0)^k\right], \quad (3)$$

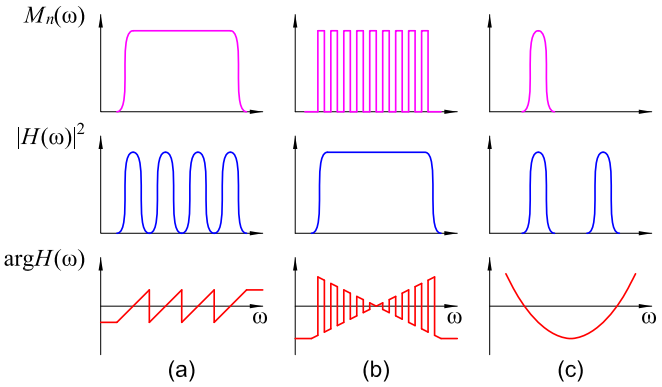

FIG. 1. Three types of transmission function $\widetilde{H}(\omega)$ corresponding to different pulse replication methods: top – mask function, middle – absolute value, bottom – phase; (a) direct phase and amplitude modulation, (b) phase-only MICS method, (c) chirped pulse modulation. The example shown is for $N = 2$ pulses at the output sequence.

where $M_n(\omega)$ is the amplitude mask function corresponding to the nth pulse in the sequence, $D_n^{(k)}$ is the kth order dispersion corresponding to the nth pulse, and $T(\omega)$ is the envelope of spectral transmission for all pulses in the sequence. The difference between one or another pulse shaping method is in particular choice of mask functions $M_n(\omega)$.

Figure 1 illustrates three different approaches to producing pulse sequences. The first one, direct phase and amplitude modulation, does not use masks, but it inserts an additional loss of approximately 50% of pulse energy [43]. The second one, known as multiple independent comb shaping (MICS), is a phase-only method that uses complimentary mask functions which cover the whole laser bandwidth [42]. Phase modulation provided by the pulse shaper is a piecewise function carrying each replica on a separate frequency comb. The third method is modulation of chirped pulses when each replica originates from its own part of the spectrum and its bandwidth is essentially narrower. This method does not preserve Fourier-transform-limited (FTL) duration of laser pulses, but it makes it possible to increase the delay between the replicas sufficiently and to obtain a large number of pulses in the sequence [34].

B. Phase-and-amplitude modulation

The first method to be analyzed is direct phase-and-amplitude shaping, which is obtained when amplitude masks are not applied, i.e., $M_n(\omega) = 1$. In practice, it is often required to provide the same dispersion for each replica, resulting in the following transmission function:

$$\widetilde{H}(\omega) = T(\omega)\exp\left[i\sum_{k\geqslant 2} D^{(k)}(\omega-\omega_0)^k\right] \times \sum_{n=1}^{N} A_n \exp(i\omega\tau_n). \quad (4)$$

In Eq. (4), both phase and amplitude of $\widetilde{H}(\omega)$ vary with the frequency ω that requires a pulse shaper capable of phase and amplitude modulation. The structure of the beatings in the shaped pulse power spectrum $|\widetilde{S}_{\text{out}}(\omega)|^2$ is determined by

the number of pulses in the sequence, their amplitudes, and relative delays. At $N = 2$ the period of the beating is inversely proportional to the delay between the pulses, $\Delta\tau = \tau_2 - \tau_1$. In the wavelength domain, the output spectrum is modulated with the period $\lambda^2/(c\Delta\tau)$. With increase in delay, the beatings become shorter and modulation depth degrades because of a limited spectral resolution of the AODDL. Actual AODDL performance is characterized by the spectral modulation transfer function [44]. Thus, maximum delay between the replicas $\Delta\tau$ is related to the passband of the AODDL, $\delta\lambda$. One can estimate it as

$$\max \Delta\tau \approx \frac{\lambda^2}{1.5\,\delta\lambda\, c}, \tag{5}$$

where the factor of 1.5 corresponds to an ideal sinc-shaped transmission function of the AODDL and the modulation depth of 0.5. In real-life experimental conditions, different factors result in distortions and broadening of the transmission function. The most important of them are laser beam divergence [45], crystal heating caused by ultrasound absorption [46], and ultrasonic field structure in crystals [47]. As a result, maximum delay between the replicas $\Delta\tau$ is also decreased.

C. Multiple independent comb shaping

In this work we focused on an alternative approach based on the MICS technique. Following Refs. [39,42], we divide the spectral window $\Delta\omega$ into a series of intervals Ω_j where j is the index that varies from 1 to QN, and Q is an integer number. Then we define spectral masks as

$$\begin{aligned} M_n(\omega) &= 1, \qquad \omega \in \Omega_{n+qN}, \\ &= 0, \qquad \omega \notin \Omega_{n+qN}, \end{aligned} \tag{6}$$

where q is an index that varies from 0 to $Q-1$. Thus we obtain N binary functions which are mutually orthogonal:

$$M_n(\omega)M_k(\omega) = 0 \quad \text{at} \quad n \neq k. \tag{7}$$

Each mask function $M_n(\omega)$ is a comb of Q rectangular teeth that corresponds to one of the pulses in the sequence. The mask functions cover the whole emission bandwidth so that

$$\sum_{n=1}^{N} M_n(\omega) = 1. \tag{8}$$

The advantage of using an AODDL for direct time-domain pulse shaping instead of a liquid crystal SLM is that the intervals Ω_j are not related to the construction of the SLM shaper and therefore they can be chosen arbitrarily. Actual limitation on the full number of intervals QN is the spectral resolution of the AODDL. In a high-resolution configuration it can be as high as $\lambda/\delta\lambda \sim 10^4$ [26]. Our previous experiments demonstrated that in the window of 120 nm more than 100 independent intervals can be formed [33]. Amplitude modulation capability of AODDL allows choosing unequal amplitudes of the replicas A_n.

Hereinafter we will consider equal spectral intervals with the width $|\Omega_j| = \Delta\omega/(QN)$. Respective wavelength interval at the center of the spectral window equals to $\Lambda = |\Omega_j|\lambda^2/(2\pi c)$. In the case of equal amplitudes, $A_n = 1$, this will be similar to a phase-only MICS shaping method [39,42].

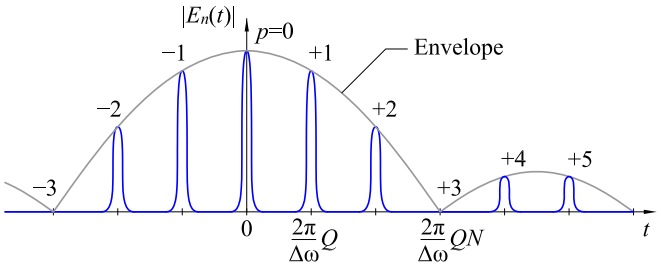

FIG. 2. Single replica pulse response of the MICS method for $N = 3$; p is the satellite number, equivalent to the principal maximum order of a diffraction grating.

Each pulse of the shaped sequence is carried by a spectral comb spread over the whole bandwidth of the input pulse. A direct analog to this method is well known diffraction of light by a grating consisting of equidistant slits with Q for the total number of slits in the grating and $N|\Omega_j| = \Delta\omega/Q$ for the period of the grating. The impulse response for the n-th replica, $\widetilde{E}_n(t)$, is a Fourier transform of the comb function. It is similar to angular intensity distribution of a periodic diffraction grating. The expression for the impulse response is

$$\begin{aligned} \widetilde{E}_n(t) = &\frac{\exp(i\,\Delta\omega t) - 1}{\exp(i\,\Delta\omega t/Q) - 1} \\ &\times \operatorname{sinc}\frac{\Delta\omega t}{2\pi\, QN} \exp\left[\frac{i\,\Delta\omega(N+n)t}{QN}\right]. \end{aligned} \tag{9}$$

Then the output complex waveform is $\widetilde{E}_{\text{out}}(t)$ is determined by a convolution of the input waveform $\widetilde{E}_{\text{in}}(t)$ and the pulse response $\widetilde{E}_n(t)$ with respect to delays and amplitudes as

$$\widetilde{E}_{\text{out}}(t) = \sum_{n=1}^{N} A_n \widetilde{E}_{\text{in}}(t) \otimes \widetilde{E}_n(t+\tau_n). \tag{10}$$

Principal features of the inpulse response (9) are illustrated in Fig. 2. The width of each interval $|\Omega_j|$ determines the sinc-shaped envelope of the impulse response. Zeros of the envelope are integer multiples of $(2\pi/\Delta\omega)QN$. Interference among the comb teeth results in a periodic function represented by the first multiplier in (9) which has principal maxima at $t = (2\pi/\Delta\omega)Qp$, where p is an integer index (similar to diffraction order index of a grating). In the pulse shaping application, principal maxima of the interference function $\widetilde{E}_n(t)$ determine satellite replicas of the pulse. The nearest satellite is separated from the central peak of the impulse response with the interval

$$\tau_{\text{sat}} = \frac{2\pi\, Q}{\Delta\omega} = \frac{2\pi}{N|\Omega_j|}. \tag{11}$$

Thus, shorter intervals $|\Omega_j|$ are preferred to increase the range of adjustable delays between the replicas.

The maximum delay between the pulses in the sequence when the replicas do not overlap with the nearest satellite can be estimated as

$$\max \Delta\tau \approx \frac{\lambda^2}{\Delta\lambda c} Q = \frac{\lambda^2}{1.5\,\delta\lambda\, c\, N}, \tag{12}$$

where the minimum width of the spectral interval $|\Omega_j|$ corresponds to the wavelength interval $\Lambda = 1.5\delta\lambda$. Thus, the

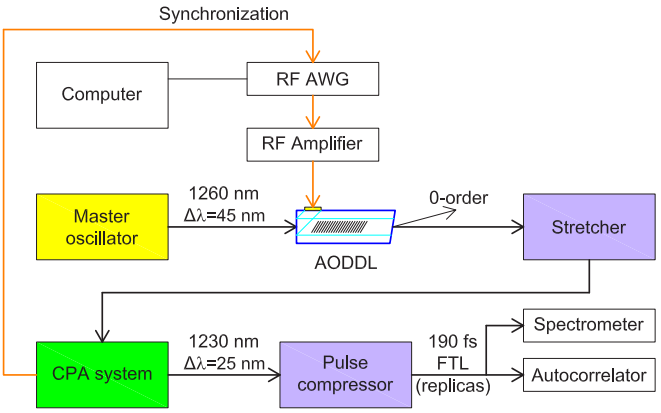

FIG. 3. Experimental setup.

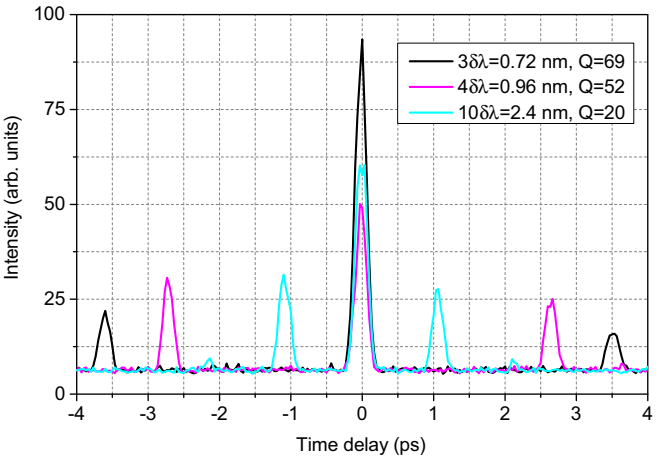

FIG. 4. Autocorrelation function of a pulse with satellites at various widths of the comb teeth.

maximum delay between the pulses in the MICS method is smaller than obtained by direct phase-and-amplitude modulation by the factor of N.

Equations (4) and (12) lead to an important conclusion that the maximum delay between the replicas is determined by the spectral resolution of the AODDL. Thus the length of acousto-optic interaction and the geometry of the interaction in the crystal are crucial for increasing the range of adjustable replica delay [45].

III. EXPERIMENTAL RESULTS AND DISCUSSION

A. Experimental setup

The experimental setup was based on a Cr:forsterite terawatt laser system [48]. The scheme of the experiment is shown in Fig. 3. The CPA system consisted of regenerative amplifier and three multipass amplifier stages. The AODDL was placed at the front end of the laser system before the stretcher. Thus, transmission losses in the AODDL were compensated by adjusting the number of passes through the regenerative amplifier. An important feature of the CPA system is a short-wavelenght spectral shift which occurs mainly in the regenerative amplifier. To measure the pulse parameters at the output of the laser system we used a scanning autocorrelator in a noncollinear geometry with the resolution of 33 fs. The FWHM of the autocorrelation function (ACF) corresponding to the 190-fs FTL pulse without shaping is equal to 0.27 ps. The AODDL was driven with a computer-controlled RF AWG and a 25 W broadband amplifier. RF waveform generation was synchronized with the CPA pump subsystem.

As we have shown above, high spectral resolution of the AODDL is the crucial parameter for obtaining a large delay between the replicas. For this reason, we used a high-resolution configuration of the paratellurite AODDL with an interaction length of 60 mm and a transmission bandwidth $\delta\lambda = 0.24$ nm at the wavelength of 1260 nm, which is 40% narrower than other reported designs of AODDL for Cr:forsterite laser systems [24]. This configuration of quasicollinear diffraction in paratellurite and the design parameters of the AODDL have been described elsewhere [26,45]. Diffraction efficiency in the experiment was up 80% on the spectral bandwidth $\Delta\lambda = 100$ nm. In the experiments, the AODDL was running in zero-dispersion mode so that negative second- and third-order dispersions of AO diffraction were added to compensate for dispersion of the paratellurite crystal. According to Eq. (5) the maximum replica delay for the parameters of the AODDL is approximately 14 ps using direct phase-and-amplitude modulation. This is almost twice less than the maximum group delay of 24 ps produced by the AODDL.

B. Pulse response measurement

In experiments, we measured performance of phase-only pulse shaping for creating precisely controlled replicas and compared performance of this method with direct phase-and-amplitude modulation. Implementation of the MICS method requires appropriate choice of the number of intervals, Q. Unlike liquid crystal SLM shapers where the only way to control the number of intervals is using pixel binning, AODDLs provide continuous control of the width and the number of the comb teeth. The processed optical bandwidth $\Delta\omega$ is also easily adjustable by software.

First, we measured the impulse response of the AODDL operating in the MICS regime setting a periodic transmission comb with the parameters $N = 2$, $A_1 = 1$, $A_2 = 0$, and the width of the comb teeth varied. The ACF in Fig. 4 shows the main pulse and the nearest satellites ($p = \pm 1$). The intervals between the main peak and the first satellite are proportional to Q and fit well Eq. (11). The intensity of the ACF side peaks decreases at $\Lambda = 3\delta\lambda$, which indicates degradation in modulation contrast owing to finite spectral resolution of the AODDL. This correlates well with our previous experiments on modulation transfer functions, which demonstrated approximately twofold difference between spectral resolution measured in the broadband modulation regime and in the single-frequency regime [44]. Further increasing the number of teeth per comb, Q, and narrowing of the tooth width Λ below actual spectral resolution of the AODDL resulted in rapid vanishing of the satellites because of low modulation contrast.

C. Generation of pulse replicas

Experiments demonstrating synthesis of $N = 2$ replicas were performed with different numbers of the comb teeth,

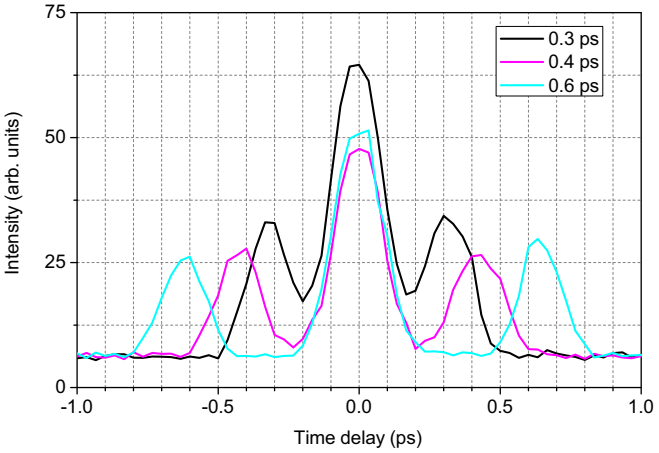

FIG. 5. Autocorrelation function of $N = 2$ replicas with various delay $\Delta\tau$ from 0.3 to 0.6 ps. The width of the comb teeth is $4\delta\lambda = 0.96$ nm, $Q = 52$.

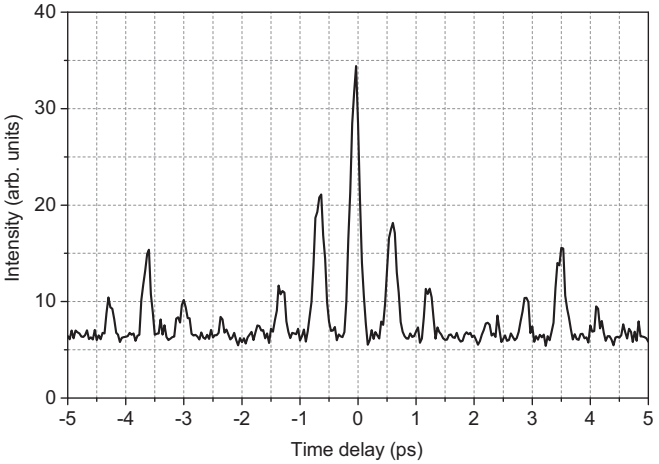

FIG. 7. Autocorrelation function of $N = 3$ replicas with equal intervals of $\Delta\tau = 0.6$ ps. The width of the comb teeth is $2\delta\lambda = 0.48$ nm, $Q = 69$.

Q. The ACF in Fig. 5 was obtained with the comb tooth width $\Lambda = 4\delta\lambda = 0.96$ nm, $Q = 52$. Experiments with the tooth width $\Lambda = 3\delta\lambda = 0.72$ nm, $Q = 69$ were qualitatively the same within experimental accuracy. We also compared the MICS method with direct phase-and-amplitude modulation according to Eq. (4) as the reference. The output energy was calculated as the integral of the spectrum in the wavelength window 1210–1250 nm. The phase-only MICS method provided 30% greater energy than the reference obtained with the phase-and-amplitude method. The spectra for $\Lambda = 4\delta\lambda = 0.96$ nm, $Q = 52$ and $\Lambda = \delta\lambda = 0.24$ nm, $Q = 208$ are shown in Fig. 6. The reference spectrum demonstrates that the gain saturation in the regenerative amplifier reduces the depth of amplitude modulation created by the AODDL. Modulation contrast at the output of the laser system was approximately 3 dB while directly measured contrast before the CPA system (at the output of the AODDL) was better than 8 dB.

Generation of $N = 3$ pulses in a sequence is presented in Fig. 7. In this experiment, the width of the comb tooth was reduced to $\Lambda = 2\delta\lambda = 0.48$ nm, so the number of teeth in each comb was $Q = 69$. The position of the first satellite according to Eq. (11) was at $\tau_{\text{sat}} = 3.6$ ps, the same as at $N = 2$ and $\Lambda = 3\delta\lambda$ tooth width.

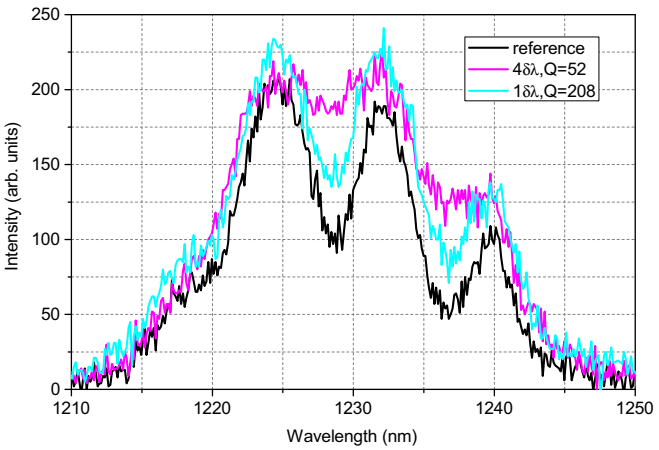

FIG. 6. Output spectra for $N = 2$ replicas with the delay $\Delta\tau = 0.6$ ps. The reference spectrum was obtained using direct phase-and-amplitude modulation.

Experimental data in Fig. 6 demonstrate modulation in output spectra when the MICS pulse shaping method is used. Modulation depth increases with the number of comb teeth Q. The explanation for this phenomenon is in finite spectral resolution of AODDL. An ideal transmission function defined by Eq (3) and (6) provides a piecewise phase modulation, but actual response of the AODDL is a convolution of $\widetilde{H}(\omega)$ with a single-frequency transmission function of the AODDL. Because of this, amplitude modulation appears in the diffracted spectrum at the phase steps of $\widetilde{H}(\omega)$. A similar effect of intensity modulation resulting from phase steps is known as phase-amplitude coupling in Fourier domain pulse shapers [49]. While the comb teeth are wide, $|\Omega_j| \gg 2\pi c\delta\lambda/\lambda^2$, the transmission function contains separate rejection bands with the typical width of the AODDL passband and depth proportional to the phase step. However, if the period of the comb becomes less than the AOTF passband, the condition of comb independency (7) cannot be satisfied any more. As a result, rejection bands in $|\widetilde{H}(\omega)|$ merge and the period of amplitude modulation becomes typical for phase-and-amplitude modulation. In the experiments, we observed spectral modulation of output emission when the comb period was less than $\Lambda = 4\delta\lambda$. In Fig. 6, separate rejection bands at the phase steps are not resolved by the spectrometer, but the large scale modulation is clearly seen. The spectrum obtained by the MICS method with the interval corresponding to $\Lambda = \delta\lambda$ does not qualitatively differ from the reference spectrum obtained by direct phase-and-amplitude modulation. Thus, the number of intervals QN corresponding to 2–3 passbands of AODDL can be considered as a practical limit for using the MICS method.

IV. SUMMARY

We demonstrated phase-only generation of femtosecond pulse sequences performed by a custom-built high-resolution

acousto-optical pulse shaper. Application of the method was studied in a terawatt CPA laser system with a highly saturated regenerative amplifier. It has been shown that phase-only pulse shaping helps to minimize optical losses and to avoid undesirable decrease of modulation depth originating from amplifier saturation when using conventional phase-and-amplitude modulation.

We consider acousto-optic pulse replication as an appropriate instrument for various scientific and engineering applications including pump-probe experiments, material processing, and generation of tunable narrowband THz radiation using optical rectification. Owing to fully electronic continuous precision adjustment of processed emission bandwidth and central wavelength, controllable replica delay, and variety of pulse shaping algorithms, an AODDL is an accurate and flexible controlling device for laser drivers producing controlled pulse sequences.

ACKNOWLEDGMENTS

The research was supported in part by the Ministry of Education and Science of the Russian Federation in the framework of Increase Competitiveness Program of National University of Science and Technology "MISIS" (Project K2-2016-072), and by the Russian Foundation for Basic Research (Project 15-07-03719). The experiments were conducted using Unique Facility "Terawatt Femtosecond Laser Complex" in the Center for Collective Usage "Femtosecond Laser Complex" of JIHT RAS and supported within the framework of the Fundamental investigation program of the Presidium of the the Russian Academy of Sciences I.31 P.

[1] A. M. Weiner, Opt. Commun. **284**, 3669 (2011).
[2] V. V. Lozovoy, I. Pastirk, E. J. Brown, B. I. Grimberg, and M. Dantus, Int. Rev. Phys. Chem. **19**, 531 (2000).
[3] A. Präkelt, M. Wollenhaupt, C. Sarpe-Tudoran, and T. Baumert, Phys. Rev. A **70**, 063407 (2004).
[4] A. Stolow, A. Bragg, and D. Neumark, Chem. Rev. **104**, 1719 (2004).
[5] T. Kim, J.-C. B. Kim, K. K. Kim, I. S. Ko, and H. Suk, Phys. Lett. A **370**, 310 (2007).
[6] B. T. Torosov and N. V. Vitanov, Phys. Rev. A **83**, 053420 (2011).
[7] G. T. Genov, D. Schraft, N. V. Vitanov, and T. Halfmann, Phys. Rev. Lett. **118**, 133202 (2017).
[8] A. Konar, J. D. Shah, V. V. Lozovoy, and M. Dantus, J. Phys. Chem. Lett. **3**, 1329 (2012).
[9] J. Roth, A. Kraus, J. Lotze, and H.-R. Trebin, Appl. Phys. A **117**, 2207 (2014).
[10] C. Kerse, H. Kalaycioglu, P. Elahi, B. Cetin, D. K. Kesim, O. Akcaalan, S. Yavas, M. D. Asik, B. Oktem, H. Hoogland *et al.*, Nature (London) **537**, 84 (2016).
[11] L. Greenman, C. P. Koch, and K. B. Whaley, Phys. Rev. A **92**, 013407 (2015).
[12] N. V. Didenko, A. V. Konyashchenko, P. V. Kostryukov, L. L. Losev, V. S. Pazyuk, S. Yu. Tenyakov, V. Ya. Molchanov, S. I. Chizhikov, and K. B. Yushkov, Quantum Electron. **45**, 1101 (2015).
[13] A. V. Konyashchenko, P. V. Kostryukov, L. L. Losev, and V. S. Pazyuk, Quantum Electron. **47**, 1 (2017).
[14] C. Manzoni, O. D. Mücke, G. Cirmi, Sh. Fang, J. Moses, Sh.-W. Huang, K.-H. Hong, G. Cerullo, and F. X. Kärtner, Laser Photonics Rev. **9**, 129 (2015).
[15] J. Ahn, A. V. Efimov, R. D. Averitt, and A. J. Taylor, Opt. Express **11**, 2486 (2003).
[16] J. Krause, M. Wagner, S. Winnerl, M. Helm, and D. Stehr, Opt. Express **19**, 19114 (2011).
[17] J. Lu, H. Y. Hwang, X. Li, S.-H. Lee, O-P. Kwon, and K. A. Nelson, Opt. Express **23**, 22723 (2015).
[18] A. V. Ovchinnikov, O. V. Chefonov, V. Ya. Molchanov, K. B. Yushkov, C. Vicario, and C. Hauri, Quantum Electron. **46**, 1149 (2016).
[19] A. Galler and T. Feurer, Appl. Phys. B **90**, 427 (2008).
[20] D. Pestov, V. V. Lozovoy, and M. Dantus, Opt. Lett. **35**, 1422 (2010).
[21] F. Verluise, V. Laude, Z. Cheng, Ch. Spielmann, and P. Tournois, Opt. Lett. **25**, 575 (2000).
[22] M. Pittman, S. Ferré, J. P. Rousseau, L. Notebaert, J. P. Chambaret, and G. Chériaux, Appl. Phys. B **74**, 529 (2002).
[23] K. Ohno, T. Tanabe, and F. Kannari, J. Opt. Soc. Am. B **19**, 2781 (2002).
[24] V. Ya. Molchanov, S. I. Chizhikov, O. Yu. Makarov, N. P. Solodovnikov, V. N. Ginzburg, E. V. Katin, E. A. Khazanov, V. V. Lozhkarev, and I. V. Yakovlev, Appl. Opt. **48**, C118 (2009).
[25] T. Oksenhendler, D. Kaplan, P. Tournois, G. M. Greetham, and F. Estable, Appl. Phys. B **83**, 491 (2006).
[26] S. I. Chizhikov, S. G. Garanin, L. V. Goryachev, V. Ya. Molchanov, V. V. Romanov, N. N. Rukavishnikov, S. V. Sokolovskii, I. N. Voronich, and K. B. Yushkov, Laser Phys. Lett. **10**, 015301 (2013).
[27] S.-W. Bahk, I. A. Begishev, and J. D. Zuegel, Opt. Commun. **333**, 45 (2014).
[28] S.Yu. Mironov, A. K. Poteomkin, E. I. Gacheva, A. V. Andrianov, V. V. Zelenogorskii, R. Vasiliev, V. Smirnov, M. Krasilnikov, F. Stephan, and E. A. Khazanov, Laser Phys. Lett. **13**, 055003 (2016).
[29] A. Monmayrant, A. Arbouet, B. Girard, B. Chatel, A. Barman, B.J. Whitaker, and D. Kaplan, Appl. Phys. B **81**, 177 (2005).
[30] L. Bei, G. I. Dennis, H. M. Miller, T. W. Spaine, and J. W. Carnahan, Prog. Quantum Electron. **28**, 67 (2004).
[31] P. Tournois, Opt. Commun. **140**, 245 (1997).
[32] F. Verluise, V. Laude, J.-P. Huignard, P. Tournois, and A. Migus, J. Opt. Soc. Am. B **17**, 138 (2000).
[33] V. Ya. Molchanov and K. B. Yushkov, Opt. Express **22**, 15668 (2014).
[34] K. B. Yushkov, V. V. Romanov, G. S. Rogozhnikov, and V. Ya. Molchanov, Opt. Lett. **41**, 5442 (2016).
[35] K. B. Yushkov and V. Ya. Molchanov, Opt. Commun. **355**, 177 (2015).
[36] S. Coudreau, D. Kaplan, and P. Tournois, Opt. Lett. **31**, 1899 (2006).
[37] S. Weber, M. Barthélemy, and B. Chatel, Appl. Phys. B **98**, 323 (2010).

[38] D. J. McCabe, D. R. Austin, A. Tajalli, S. Weber, I. A. Walmsley, and B. Chatel, J. Opt. Soc. Am. B **28**, 58 (2011).
[39] A. M. Weiner, J. P. Heritage, and E. M. Kirschner, J. Opt. Soc. Am. B **5**, 1563 (1988).
[40] A. M. Weiner, Rev. Sci. Instrum. **71**, 1929 (2000).
[41] A. Rundquist, A. Efimov, and D. H. Reitze, J. Opt. Soc. Am. B **19**, 2468 (2002).
[42] D. Pestov, V. V. Lozovoy, and M. Dantus, Opt. Express **17**, 14351 (2009).
[43] M. M. Wefers and K. A. Nelson, J. Opt. Soc. Am. B **12**, 1343 (1995).
[44] K. B. Yushkov and V. Ya. Molchanov, Opt. Lett. **38**, 3578 (2013).
[45] V. Ya. Molchanov, V. B. Voloshinov, and O. Yu. Makarov, Quantum Electron. **39**, 353 (2009).
[46] S. A. Tretiakov, A. I. Kolesnikov, I. A. Kaplunov, R. M. Grechishkin, K. B. Yushkov, and E. V. Shmeleva, Int. J. Thermpthys **37**, 6 (2016).
[47] S. N. Mantsevich, V. Ya. Molchanov, K. B. Yushkov, V. S. Khorkin, and M. I. Kupreychik, Ultrason. **78**, 175 (2017).
[48] M. B. Agranat, S. I. Ashitkov, A. A. Ivanov, A. V. Konyashchenko, A. V. Ovchinnikov, and V. E. Fortov, Quantum Electron. **34**, 506 (2004).
[49] C. Dorrer and F. Salin, IEEE J. Sel. Top. Quantum Electron. **4**, 342 (1998).